RESEARCH ARTICLE

WILEY

Mapping white matter maturational processes and degrees on neonates by diffusion kurtosis imaging with multiparametric analysis

Xianjun Li[1] | Mengxuan Li[1] | Miaomiao Wang[1] | Fan Wu[1] | Heng Liu[1,2] | Qinli Sun[1,2] | Yuli Zhang[1] | Congcong Liu[1] | Chao Jin[1] | Jian Yang[1,2]

[1]Department of Radiology, The First Affiliated Hospital of Xi'an Jiaotong University, Xi'an, China

[2]Department of Biomedical Engineering, The Key Laboratory of Biomedical Information Engineering of the Ministry of Education, School of Life Science and Technology, Xi'an Jiaotong University, Xi'an, China

Correspondence
Jian Yang, Professor, Department of Radiology, The First Affiliated Hospital of Xi'an Jiaotong University, Xi'an, China.
Email: yj1118@mail.xjtu.edu.cn

Abstract

White matter maturation has been characterized by diffusion tensor (DT) metrics. However, maturational processes and degrees are not fully investigated due to limitations of univariate approaches and limited specificity/sensitivity. Diffusion kurtosis imaging (DKI) provides kurtosis tensor (KT) and white matter tract integrity (WMTI) metrics, besides DT metrics. Therefore, we tried to investigate performances of DKI with the multiparametric analysis in characterizing white matter maturation. Developmental changes in metrics were investigated by using tract-based spatial statistics and the region of interest analysis on 50 neonates with postmenstrual age (PMA) from 37.43 to 43.57 weeks. Changes in metrics were combined into various patterns to reveal different maturational processes. Mahalanobis distance based on DT metrics ($D_{M,DT}$) and that combing DT and KT metrics ($D_{M,DT-KT}$) were computed, separately. Performances of $D_{M,DT-KT}$ and $D_{M,DT}$ were compared in revealing correlations with PMA and the neurobehavioral score. Compared with DT metrics, WMTI metrics demonstrated additional changing patterns. Furthermore, variations of $D_{M,DT-KT}$ across regions were in agreement with the maturational sequence. Additionally, $D_{M,DT-KT}$ demonstrated stronger negative correlations with PMA and the neurobehavioral score in more regions than $D_{M,DT}$. Results suggest that DKI with the multiparametric analysis benefits the understanding of white matter maturational processes and degrees on neonates.

KEYWORDS
development, diffusion kurtosis imaging, Mahalanobis distance, neonate, white matter maturation

1 | INTRODUCTION

White matter maturation, accompanied with structural changes, underpins development of cognitive functions and behaviors (Gilmore, Knickmeyer, & Gao, 2018). Structural changes are extremely rapid during the neonatal period (Dubois et al., 2014; Ouyang, Dubois, Yu, Mukherjee, & Huang, 2019). Many neurobehavioral disorders originate from perturbations of typical maturational processes in this early period, which would lead to lower maturational degrees (Suzuki, 2007). Therefore, assessing maturational processes and degrees on neonates is essential for understanding the typical brain development and relevant disorders (Geng et al., 2012; Ouyang et al., 2019; Suzuki, 2007).

Magnetic resonance imaging (MRI) allows investigation of white matter maturational processes in vivo. The myelin water fraction and the magnetization transfer MRI can provide quantitative metrics for assessing myelination (Dubois et al., 2014; Ouyang, Jeon, et al., 2019). However, it is difficult to fully characterize maturational processes including but not limited to myelination (Paus, 2010). Sensitive to microstructural alterations, diffusion tensor imaging (DTI) is feasible to provide various diffusion tensor (DT) derived metrics, for example, axial diffusivity (AD), radial diffusivity (RD), and fractional anisotropy (FA) (Ouyang, Jeon, et al., 2019). Changes of these metrics have been thought to be related to white matter maturational processes (e.g., premyelination, myelination, etc.) (Dubois et al., 2008, 2014; Ouyang, Jeon, et al., 2019). Note that premyelination and myelination mainly focus on the development of oligodendrocytes. Actually, the axon itself undergoes dramatic changes (Paus, 2010). The axonal growth is accompanied with more organized neurofilaments, in addition to the increasing neighbor spacing of neurofilaments, decreasing density of the microtubule and mitochondria, and the increasing axoplasmic flow (Andrews et al., 2006; Garcia et al., 2003; Stassart, Möbius, Nave, & Edgar, 2018; Suzuki, Matsuzawa, Kwee, & Nakada, 2003). These alterations would increase the intra-axonal axial diffusivity ($D_{\text{a,axial}}$) (Garcia et al., 2003; Lee, Papaioannou, Kim, Novikov, & Fieremans, 2020; Suzuki et al., 2003). It is difficult for DTI to distinguish diffusion in the intra-axonal space from that in the extra-axonal space (Paus, 2010). Several models have been proposed to link the diffusion weighted signals to intra-axonal and extra-axonal structural properties, for example, the neurite orientation dispersion and density imaging (NODDI) (Zhang, Schneider, Wheeler-Kingshott, & Alexander, 2012). However, the intra-cellular diffusivity parallel to each sub-bundle in this model is set equal to each other and fixed to a predefined value (Jelescu et al., 2015; Zhang et al., 2012). This limits its ability to investigate developmental changes in $D_{\text{a,axial}}$. White matter tract integrity (WMTI) metrics derived from diffusion kurtosis imaging (DKI) may overcome this limitation by providing the estimation of $D_{\text{a,axial}}$, as well as axonal water fraction (AWF), fiber dispersion (FD), extra-axonal axial diffusivity ($D_{\text{e,axial}}$), extra-axonal radial diffusivity ($D_{\text{e,radial}}$), and tortuosity (Fieremans, Jensen, & Helpern, 2011; Jelescu et al., 2015). Therefore, this study hypothesizes that combing changes in WMTI and DT metrics may help in revealing more detailed maturational processes on neonatal white matter.

Typically, brain reaches its mature stage when measurements match the mature reference (Somerville, 2016). Accordingly, the maturational degree of white matter refers to the degree of similarity between the developing brain and the mature reference. Though MRI parametric values can reveal developmental changes on neonatal brains (Dean III et al., 2017; Gilmore et al., 2007; Hüppi et al., 1998; Kunz et al., 2014), the parametric value on the developing brain itself may be not able to reflect the maturational degree without the mature reference (Kulikova et al., 2015). Moreover, univariate approach based on one single metric (e.g., AD or RD) may not be able to reflect fully maturational degrees. It is necessary to use multivariate approaches and to take the mature brain as the reference. Multivariate techniques are often based on the measurement of distances between objects. The most commonly used distance measures are Euclidean and Mahalonobis distances (Maesschalck, Jouan-Rimbaud, & Massart, 2000). In the Euclidean distance calculation, different metrics are equally weighted. However, different MRI metrics hold different scales. As comparisons, Mahalonobis distance is the distance between a point and a distribution, which holds the advantage in characterizing the maturational degree by scaling the contribution of variables according to the variability of each variable (Ghorbani, 2019). Specifically, Mahalanobis distance based on the combination of various metrics has demonstrated greater discrimination among individuals and better characterization of maturation than univariate approaches (Dean III et al., 2017; Kulikova et al., 2015; Lindemer et al., 2015). Furthermore, among various distance measures, the Mahalanobis distance demonstrates great sensitivity to reveal the association with intelligence (Shehzad et al., 2014). Taking the mature adult brain as the reference, the smaller the distance, the closer the developing brain to the mature brain (Kulikova et al., 2015). Therefore, Mahalanobis distance is an alternative strategy to quantify maturational degrees. DT metrics have been demonstrated suitable to be included into the Mahalanobis distance calculation for assessing white matter maturation (Kulikova et al., 2015), as each metric changes in one direction to the mature reference (increasing FA, decreasing AD and RD) during the postnatal period (Dubois et al., 2014). As an extension of DTI, DKI can provide kurtosis tensor (KT) metrics (e.g., axial kurtosis, AK; radial kurtosis, RK; mean kurtosis, MK), besides DT metrics, for characterizing brain structural changes (Grinberg et al., 2017; Jelescu et al., 2015; Paydar et al., 2014). However, whether KT metrics could improve the performance of the Mahalanobis distance in quantifying maturational degrees remains to be investigated.

According to the above considerations, this study tried to investigate performances of DKI with the multiparametric analysis in characterizing white matter maturational processes and degrees on term neonates. Age-related changes in metrics were investigated by using tract-based spatial statistics (TBSS) (Smith et al., 2006) and the region of interest (ROI) analysis. Then, change patterns were assessed by combing changes of different metrics to reveal maturational processes. To quantify maturational degrees, Mahalanobis distances based on DT metrics ($D_{\text{M,DT}}$) and the combination of DT and KT metrics ($D_{\text{M,DT-KT}}$) were computed, considering the adult brain as the reference. Finally, performances of $D_{\text{M,DT-KT}}$ and $D_{\text{M,DT}}$ were compared

in revealing correlations with the postmenstrual age (PMA) and the neurobehavioral score.

2 | MATERIALS AND METHODS

This study was approved by the local institutional review board. Informed written consents were obtained from adult participants and parents of neonates.

2.1 | Participants

This study included term neonates who met the following inclusion criteria: (a) postnatal age at MRI ≤28 days; (b) term birth (gestational age ≥ 37 weeks); (c) complete MRI data; and (d) accomplished neonatal behavioral neurological assessment. Exclusion criteria were: (a) MRI abnormalities or diseases that may affect white matter maturation (e.g., punctate white matter lesions, hypoxic–ischemic encephalopathy, neonatal asphyxia, congenital heart disease, neonatal respiratory distress syndrome, etc.); (b) abnormal neurodevelopment assessed by the follow-up Bayley scales of infant development assessment (second edition, score of mental development index or psychomotor development index <85); and (c) motion artifacts.

To link Mahalanobis distance to the maturational degree, the reference should be the mature brain. As age has impacts on structural changes in the brain, adults in the plateau period may be candidates of the reference. For DT and KT metrics, changes reach a plateau in late adolescence or in the twenties (Das, Wang, Bing, Bhetuwal, & Yang, 2017; Paydar et al., 2014; Tamnes et al., 2010). Therefore, this study selected the adult as the reference. Healthy adult volunteers were recruited among students from the local university. MRI was performed on these volunteers after obtaining informed written consents and accomplishing neurological and psychiatric examinations. The inclusion criteria for adults were: (a) 18 years ≤ age at MRI < 30 years; (b) term birth (gestational age ≥ 37 weeks); (c) complete MRI data; (d) right-handed; (e) free of neurological/psychiatric diseases, without MRI abnormalities, Wechsler adult intelligence scale >85, Hamilton depression scale <7; (f) no history of brain injuries or drug/ alcohol abuse; and (g) self-reported habitual good sleep (>7 hr per night) in 2 weeks prior to the MRI scanning. Data with motion artifacts would be excluded.

2.2 | Data acquisition

MRI was performed on a 3 T scanner (Signa HDxt; GE Healthcare; Milwaukee, Wisconsin) with an 8-channel head coil. To complete the MRI examination and reduce motion artifacts, neonates were suggested to adjust the sleep habit. Subjects who could not successfully accomplish the MRI examination under the natural sleep status after three attempts or request by their parents were sedated (Phenobarbital, 4 mg/kg, intramuscular injection) after consultation

with anesthesiologists. The patient selection, monitoring, and management were performed following guidelines for pediatric patients during and after sedation (Coté & Wilson, 2006). No adverse events related to the sedation occurred during the followed-up investigation. The body temperature, the heart rate, the respiration rate, and the transcutaneous oxygen saturation were monitored throughout the MRI procedure. Micro-earplugs were placed bilaterally in the external auditory meatus of subjects to protect their hearing.

DKI was performed by using a single shot echo planar imaging sequence with following parameters: b values = 0, 500, 1,000, 2,000, 2,500 s/mm^2; 5 volumes of b = 0 s/mm^2 (b_0) (including one reversed phase-encode b_0); 18 gradient directions per nonzero b value; NEX = 1; repetition time/echo time = 11,000/91.7 ms; slice thickness = 4 mm; field of view = 180 × 180 mm^2 for neonates and 240 × 240 mm^2 for adults; acquisition matrix =128 × 128 for neonates and 172 × 172 for adults to keep the same spatial resolution; the acquisition voxel size = 1.4 × 1.4 × 4 mm^3. The acquisition time of DKI was 14 min 6 sec.

The neurobehavioral assessment was performed on neonates within 5 days before or after MRI by using the neonatal behavioral neurological assessment (Chinese) (Bao, Yu, Li, & Zhang, 1991). This assessment (including 20 items) is a composite measure based on the Chinese practice and the representative behavioral neurological measurement methods proposed by Amiel-Tison and Brazelton (Amiel-Tison et al., 1982; Brazelton, 1984). The neurobehavioral score (sum of 20 items) in this current work reflects the broad behavioral development of neonates.

2.3 | Data processing

During the data exclusion procedure, the detection of motion artifacts was performed by using an automatic method (Appendix S1) (Li et al., 2014). Taking b_0 image as the reference, images in different gradient directions were checked slice by slice using the two-dimensional local Pearson correlation coefficient. The threshold for motion artifacts detection and exclusion was set to be the SD by a factor of 3 from the average of correlation coefficients (averaged threshold = 0.81). Artifacts were detected with relatively low correlation coefficients (Figure S1). At least 2 nonzero b values and 15 gradient directions per nonzero b value should be retained to estimate the KT after the artifacts removal (Tabesh, Jensen, Ardekani, & Helpern, 2011). Geometric distortion correction was performed based on pairs of b_0 images (b_0 and the reversed phase-encode b_0) by using the topup tool (https://fsl.fmrib.ox.ac.uk/fsl/fslwiki/topup). The eddy current correction was performed for diffusion weighted images in DKI by using the eddy_correct tool of FMRIB software library (FSL, version 5.0.9) (Jenkinson, Beckmann, Behrens, Woolrich, & Smith, 2012). Then, the brain was extracted by using the FSL brain extraction tool (https://fsl.fmrib.ox.ac.uk/fsl/fslwiki/BET) (Smith, 2002). Diffusion weighted images were smoothed by using a Gaussian kernel to reduce the impact of noise and misregistration (Tabesh et al., 2011). DT and KT were estimated by using a

constrained weighted linear least squares method (Tabesh et al., 2011; Veraart et al., 2011). FA, mean diffusivity (MD), AD, and RD were derived from DT. AK, RK, and MK were calculated based on the combination of DT and KT (Cheung et al., 2009). For the estimation of WMTI metrics, AWF was calculated based on the maximum kurtosis (K_{max}) over 10,000 directions randomly chosen by using MATLAB (version 7.11; MathWorks; Natick, Massachusetts) (Fieremans et al., 2011):

$$AWF = \frac{K_{max}}{K_{max} + 3}, \tag{1}$$

Subsequently, intra-axonal diffusivities were estimated by (Fieremans et al., 2011):

$$D_{a,i} = D_i \left[1 - \sqrt{\frac{K_i(1-f)}{3f}} \right], \tag{2}$$

where, D_i and K_i were the diffusivity and kurtosis in the corresponding direction (i), while f represented the AWF. $D_{a,axial}$ was the maximum eigenvalue of the intra-axonal diffusion tensor. FD was estimated by (Jelescu et al., 2015):

$$FD = \frac{D_{a,axial}}{Tr(D_a)}, \tag{3}$$

where, $Tr(D_a)$ indicated the trace of the intra-axonal diffusion tensor. Extra-axonal diffusivities were estimated by (Fieremans et al., 2011):

$$D_{e,i} = D_i \left[1 + \sqrt{\frac{K_i f}{3(1-f)}} \right]. \tag{4}$$

$D_{e,axial}$ was the primary eigenvalue of the extra-axonal diffusion tensor. $D_{e,radial}$ was calculated by averaging the second and the third eigenvalues of the extra-axonal diffusion tensor. And the tortuosity of the extra-axonal space was calculated by:

$$Tortuosity = \frac{D_{e,axial}}{D_{e,radial}}. \tag{5}$$

The artifacts detection and the tensor estimation were performed by using an in-house program implemented in MATLAB.

Spatial normalization for neonates: Firstly, this study created the FA template for local neonates by using a group-wise method (detailed steps were provided in the Appendix S1) (Li, Gao, Wang, Wan, & Yang, 2016; Oishi et al., 2011). FA maps of neonates were normalized to the local neonatal FA template by using the combination of linear and nonlinear registrations (Ball et al., 2010; Li et al., 2016). During the procedure of registration, FMRIB's linear image registration tool (https://fsl.fmrib.ox.ac.uk/fsl/fslwiki/FLIRT) and nonlinear image registration tool (https://fsl.fmrib.ox.ac.uk/fsl/

fslwiki/FNIRT) were used. Prior to the linear registration with 12 degrees-of-freedom, applying a linear registration with 6 degrees-of-freedom would reduce registration errors (Ball et al., 2010; Li et al., 2016). Therefore, this study used both 6 and 12 degrees-of-freedom linear registrations, followed by the nonlinear registration. Other metrics were normalized into the template space by using deformation parameters of FA. The white matter skeleton, the tract center, was extracted from the mean FA map of neonates by a FA threshold of 0.15 (Ball et al., 2010; Smith et al., 2006). All the metric images were projected onto this skeleton.

Spatial normalization for adults: It is difficult to map neonatal and adult images to one common coordinate space directly. This study acquired datasets on toddlers (the participant information was provided in the Appendix S1) as the bridge for the normalization of neonates and adults. This study also created FA templates (Figure S2) for toddlers and adults, separately, by using the group-wise method (detailed steps were provided in the Appendix S1) (X. Li et al., 2016; Oishi et al., 2011). Original FA maps were normalized to their corresponding templates by using the combination of linear and nonlinear registrations (Ball et al., 2010; Li et al., 2016). To transform individual images into one common space, the FA template of neonates was firstly registered to that of toddlers, and then to that of adults by using a step-wise strategy (Figure S2) (Geng et al., 2012; Shi et al., 2011). Then, FA maps of adults were back registered to the toddler template space, and finally to the neonate template space by using the inversed transformation. Other metrics were normalized into the common space by using deformation parameters of FA. The mean FA skeleton for adults was not created independently. To keep consistency of the location between adults and neonates, metrics of adults were projected onto the mean FA skeleton of neonates.

White matter ROIs were obtained by warping the JHU White-Matter Tractography Atlas in FSL (http://fsl.fmrib.ox.ac.uk/fsl/fslwiki/Atlases). FA template available in FSL was back registered to the local FA template of adults, then to that of toddlers, and finally to that of neonates (Figure S2). White matter tracts labels corresponding to the FA template were successively warped to the template space for neonates by using deformation parameters of the FA template. Prior to the back registration, JHU-ICBM-labels was used to segment the corticospinal tract (CST) into cerebral peduncle (CST_CP), internal capsule (CST_IC), and corona radiata (CST_CR) parts. ROIs included projection tracts: bilateral CST_CP, CST_IC, and CST_CR; commissural tracts: forceps major (F_major) and forceps minor (F_minor); association tracts: bilateral inferior longitudinal fasciculus (ILF) and superior longitudinal fasciculus (SLF). ROIs were defined as the overlap between warped labels and the white matter skeleton. WMTI model is applicable in regions with relatively aligned fibers and the angular spread of ≤30°. To satisfy this condition, the current work performed analyses for WMTI metrics on voxels with FD ≥0.75 (corresponding to angle ≤30°) on the FA skeleton (Figure S3) (Fieremans et al., 2011; Jelescu et al., 2015).

Mahalanobis distance calculation: To quantify maturational degrees, Mahalanobis distances between neonatal and adult brains were calculated on the white matter skeleton in the neonatal template space by using the following equation:

$$\text{Mahalanobis distance} = \sqrt{(x-\mu)^{T}S^{-1}(x-\mu)}, \qquad (6)$$

where x was a multivariate vector in each voxel of the neonatal white matter, μ and S were the mean vector and covariance matrix for metrics of the same voxel on adult brains. Prior to the calculation of the Mahalanobis distance, possible age effects on metrics of adults were investigated. As shown in the Figure S4 and Table S1, no significant correlation between age and metrics of adults. During the calculation of the Mahalanobis distance, "independent" metrics (e.g., AD, RD, AK, RK, etc.) could provide complementary information and are necessary to be included (Kulikova et al., 2015). As for DT metrics, MD is a linear combination of AD and RD: MD = (AD + 2RD)/3. Compared with AD and RD, MD did not provide additional information for revealing maturational changes (Figure S5). Additionally, including FA or MD did not improve the performance of the Mahalanobis distance (Figure S6). WMTI metrics were valid only in limited regions. Therefore, FA, MD and WMTI metrics were not included in the Mahalanobis distance calculation. As for KT metrics, MK could provide additional information, compared with AK and RK (Nørhøj Jespersen, 2018). Figure S6 showed that including MK into the calculation of the Mahalanobis distance would improve performances in reflecting correlations with PMA and the neurobehavioral score. Note that Mahalanobis distance based on the combination of DT and KT metrics holds better performance than that based on just DT or KT metrics (Figure S6D). This indicates that DT and KT metrics provide complementary information for assessing white matter maturation. Finally, Mahalanobis distances in this work were calculated by using "independent" DT metrics (AD and RD) and the combination of DT and KT metrics (AD, RD, AK, RK, and MK), named $D_{M,DT}$ and $D_{M,DT\text{-}KT}$, separately.

2.4 | Statistical analysis

Relationships between DT, KT, WMTI metrics and PMA were performed by using the general linear model while adjusting for covariates of the gender and the birth weight in TBSS (Smith et al., 2006; Winkler, Ridgway, Webster, Smith, & Nichols, 2014). The family-wise error rate correction and the threshold-free cluster enhancement were performed for tests in TBSS (Smith & Nichols, 2009). As shown in the Figure S3, voxels with FD ≥0.75 mainly locate in bilateral CST_IC and F_major. Therefore, the ROI analysis for age-related changes in metrics was performed in bilateral CST_IC and F_major. Correlations between regional values of DT, KT, WMTI metrics and PMA were performed by using the partial Spearman correlation while controlling for effects of the gender and the birth weight. Determination coefficients (R^2) of different methods (including linear, logarithmic, and exponential methods) for fitting PMA-related changes in DT, KT, and WMTI metrics were compared. As shown in the Figure S7, there was no significant difference in R^2 across these three fitting methods. Therefore, linear trend lines were used to reveal PMA-related changes in DT, KT, and WMTI metrics.

It is not possible to infer the maturational process based on one single metric (Jones, Knösche, & Turner, 2013). Therefore, this study

provided change patterns, that is, combinations of changes in different metrics. Changes in metrics were determined by using the TBSS. Prior to the combination of these changes, p values during multiple comparisons across different metrics were adjusted by using the false discovery rate correction. The age-related changes in DT, KT, and WMTI metrics were combined into different change patterns (taking DT metrics as example, Pattern 1: decreased AD, decreased RD, and unchanged/increased FA; Pattern 2: unchanged AD, decreased RD, and increased FA; etc.). To demonstrate the asynchrony of maturation in each tract, the volume proportion of each pattern relative to the whole ROI volume (in percentage) within one ROI was calculated by:

$$\text{Proportion} = 100\% \times \frac{\text{Voxel number of pattern}_{i}}{\text{Voxel number of ROI}}, \qquad (7)$$

where pattern_i represents the ith pattern. This proportion would also help to reveal the main maturational changing pattern in each tract. Proportions of change patterns across different ROIs were tested by using the Chi-square test in SPSS (version 17; SPSS Inc.; Chicago, Illinois).

To compare regional values between $D_{M,DT}$ and $D_{M,DT\text{-}KT}$, the Wilcoxon signed rank test in SPSS was performed in each ROI. After the inter-hemisphere comparison, the asymmetry index was calculated by:

$$\text{Asymmetry index} = \frac{\text{Right} - \text{Left}}{0.5 \times (\text{Right} + \text{Left})}. \qquad (8)$$

Voxel-wise and ROI-wise correlations between Mahalanobis distances and PMA were performed by using the partial Spearman correlation while controlling for effects of the gender and the birth weight. Partial Spearman correlation was used to test correlations between Mahalanobis distances and the neurobehavioral score after controlling PMA, the gender and the birth weight. To determine the fitting method for revealing PMA-related and neurobehavioral score-related changes in Mahalanobis distances, R^2 of linear, logarithmic, and exponential methods were also calculated. Exponential fitting method held relatively higher R^2 than linear and logarithmic fitting methods (Figure S8). Therefore, the exponential fitting method was used to reveal PMA-related and neurobehavioral score-related changes in Mahalanobis distances.

The p values during multiple comparisons (across different metrics and regions) were adjusted by using the false discovery rate correction. Tests were considered statistically significant at $p < .05$ after the multiple comparison correction.

3 | RESULTS

3.1 | Demographics

According to the inclusion and exclusion criteria, this study enrolled 50 term neonates (males/females, 34/16; birth weight, 3.21 ± 0.45 kg) with PMA from 37.43 to 43.57 weeks (40.48

± 1.43 weeks), gestational age from 37.00 to 42.14 weeks (39.14 ± 1.31 weeks), postnatal age at MRI from 1 to 26 days (9.40 ± 5.16 days), neonatal neurobehavioral score from 29 to 37 (34.34 ± 2.40). Meanwhile, 30 adults (males/females, 13/17) with postnatal age from 18.92 to 26.92 years (22.78 ± 1.46 years) were enrolled as the reference for the calculation of Mahalanobis distances.

3.2 | Representative parametric maps

Representative parametric maps (DT, KT, and WMTI metrics) of a neonate, an adult, and median maps in the template space were shown in Figure 1. These parametric maps demonstrated contrast differences across metrics. Meanwhile, tremendous differences could be found between parametric maps of the neonate and those of the adult. Furthermore, differences across white matter regions could also be found, especially on neonatal parametric maps. Specifically, CST_IC and F_major held higher regional values in AD, FA, AK, RK, MK, AWF, $D_{a,axial}$, FD, $D_{e,axial}$, and Tortuosity, while lower regional values in RD and $D_{e,radial}$.

3.3 | DT, KT, and WMTI metrics: PMA-related changes and combination patterns

3.3.1 | PMA-related changes

With the increase of PMA, changes in DT metrics (decreasing AD, decreasing RD, and increasing FA) could be found on almost the whole white matter skeleton, except for corpus callosum and CST (Figure 2). As comparisons, KT (increasing RK and MK) revealed additional structural alterations on parts of corpus callosum and CST. Compared with DT metrics, WMTI extra-axonal metrics showed similar change styles in voxels with FD ≥0.75: unchanged $D_{a,axial}$, decreasing $D_{e,radial}$, and increasing tortuosity (Figure 2: AD vs. $D_{e,axial}$, RD vs. $D_{e,radial}$, FA vs. Tortuosity). AWF and intra-axonal WMTI metrics provided complementary information: increasing AWF, increasing $D_{a,axial}$, increasing FD.

As for the ROI analysis, structural alterations on left and right CST_IC occurred mainly in the radial direction (RD, RK, and $D_{e,radial}$), while no significant changes could be observed in AD, AK, and $D_{e,axial}$ (Figure 3). In the axial direction, significant increase could found in $D_{a,axial}$. Similarly, PMA-related increase in $D_{a,axial}$ was also observed on F_major, though changes in AD, RD, AK, FD, $D_{e,axial}$, and $D_{e,radial}$ were not significant (Figure 3c).

3.3.2 | Combination patterns of PMA-related changes

Based on PMA-related changes in DT metrics, five combination patterns could be found on the neonatal white matter (Figure 4a). Main parts (Table S2, volume proportion: 62–90%) of CST_CR, F_major, F_minor, ILF, and SLF underwent synchronously decreased AD and RD, while main parts of left and right CST_IC (volume proportion: 85% on the left and 63% on the right) underwent unchanged AD and decreased RD. Combination of PMA-related changes in KT metrics revealed three patterns (Figure 4b). Except for regions without significant changes, main parts of white matter underwent unchanged AK, increased RK and MK (Figure 4b). In regions with FD ≥0.75, four patterns were revealed by changes of AWF and intra-axonal metrics, while two patterns by changes of extra-axonal metrics (Figure 4c). ROI analysis demonstrated that the spatial distribution of combination patterns for changes in extra-axonal WMTI metrics was similar to that of DT metrics (Figure 3). Furthermore, AWF and intra-axonal WMTI metrics demonstrated additional change patterns. ROI analysis revealed that left CST_IC, right CST_IC, and F_major underwent synchronous PMA-related increases in AWF and $D_{a,axial}$ without significant changes in FD.

3.4 | Mahalanobis distances: Regional values and correlations with PMA, neurobehavioral score

### 3.4.1 | Regional values of $D_{M,DT-KT}$ and $D_{M,DT}$

Higher $D_{M,DT-KT}$ than $D_{M,DT}$ could be observed in all the investigative white matter regions (Figure 5a,b). Mahalanobis distance maps and the ROI analysis also showed that regional values in $D_{M,DT}$ and $D_{M,DT-KT}$ varied across white matter tracts. According to regional values in $D_{M,DT}$, CST_IC held lower $D_{M,DT}$ than CST_CP. According to regional values in $D_{M,DT-KT}$, the maturational sequence of the projection tracts from lower to higher $D_{M,DT-KT}$ was as follows: left CST_CP, right CST_CP, left CST_IC, right CST_IC, left CST_CR, right CST_CR; commissural tracts: F_major, F_minor; association tracts: left ILF, right ILF, left SLF, and right SLF. Furthermore, projection tracts of left and right CST_CP held lower $D_{M,DT-KT}$ than commissural and association tracts. Additionally, asymmetry indices for CST_CP, CST_IC, ILF, and SLF demonstrated left lateralization (Figure 5c, asymmetry index >0, left tracts held lower $D_{M,DT-KT}$ than the right), while the difference in $D_{M,DT-KT}$ between left and right CST_CR was not significant.

3.4.2 | Correlation with PMA

Negative correlation could be found between Mahalanobis distances and PMA (Figure 6 and Figure S9). As shown in TBSS results (Figure 6a), $D_{M,DT-KT}$ demonstrated more areas (e.g., genu and body of corpus callosum) with significant correlation than $D_{M,DT}$. Importantly, absolute values of correlation coefficients revealed by $D_{M,DT-KT}$ (r: −.32 to −.68) were higher than those revealed by $D_{M,DT}$ (r: −.23 to −.56) (Figure S9). Relatively stronger correlation could be found on projection and association tracts (e.g., corona radiate and external capsule) (indicated by arrows in Figure 6a).
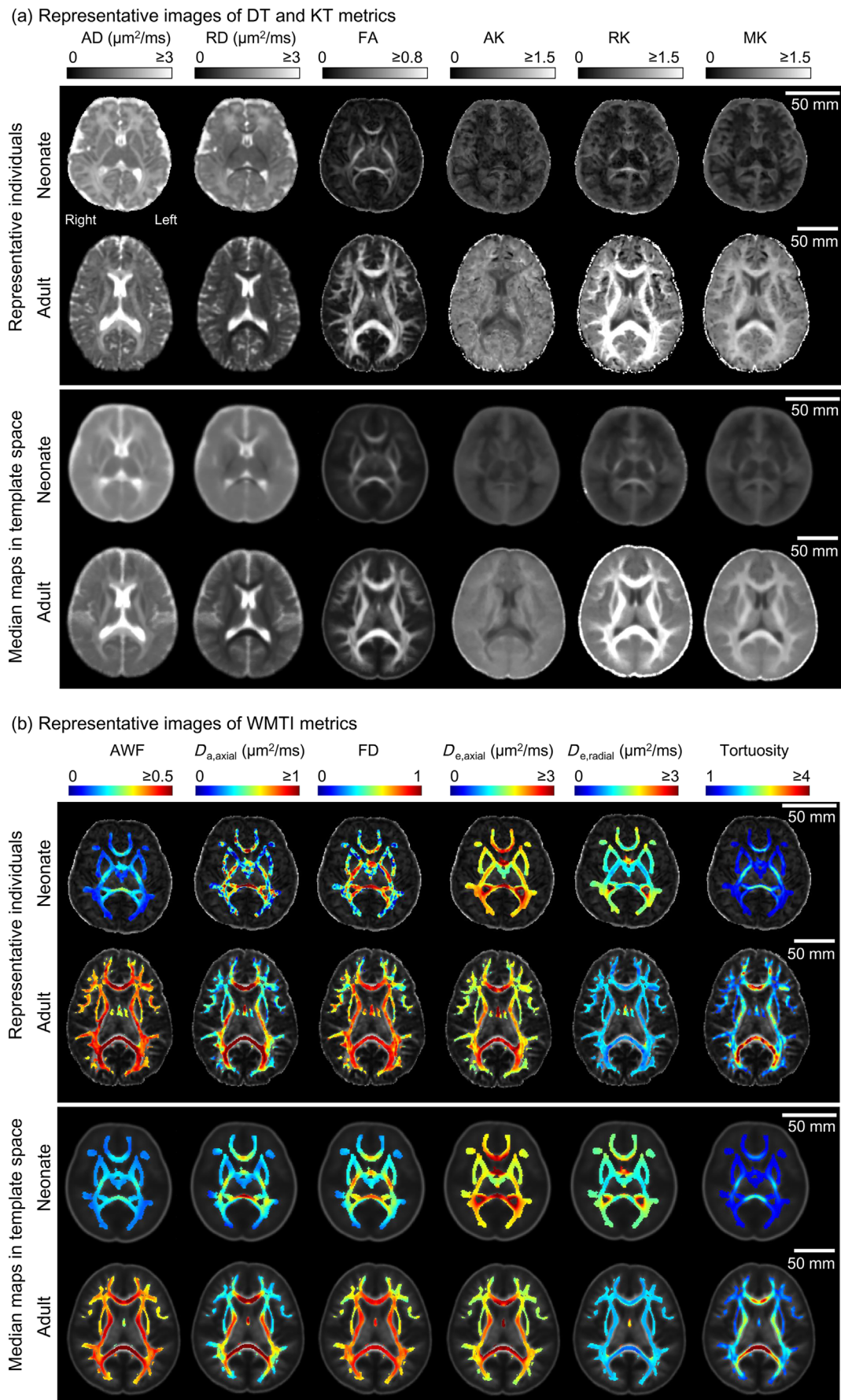
FIGURE 1 (a,b) Representative images of DT, KT, and WMTI metrics. DT, diffusion tensor; KT, kurtosis tensor; WMTI, white matter tract integrity
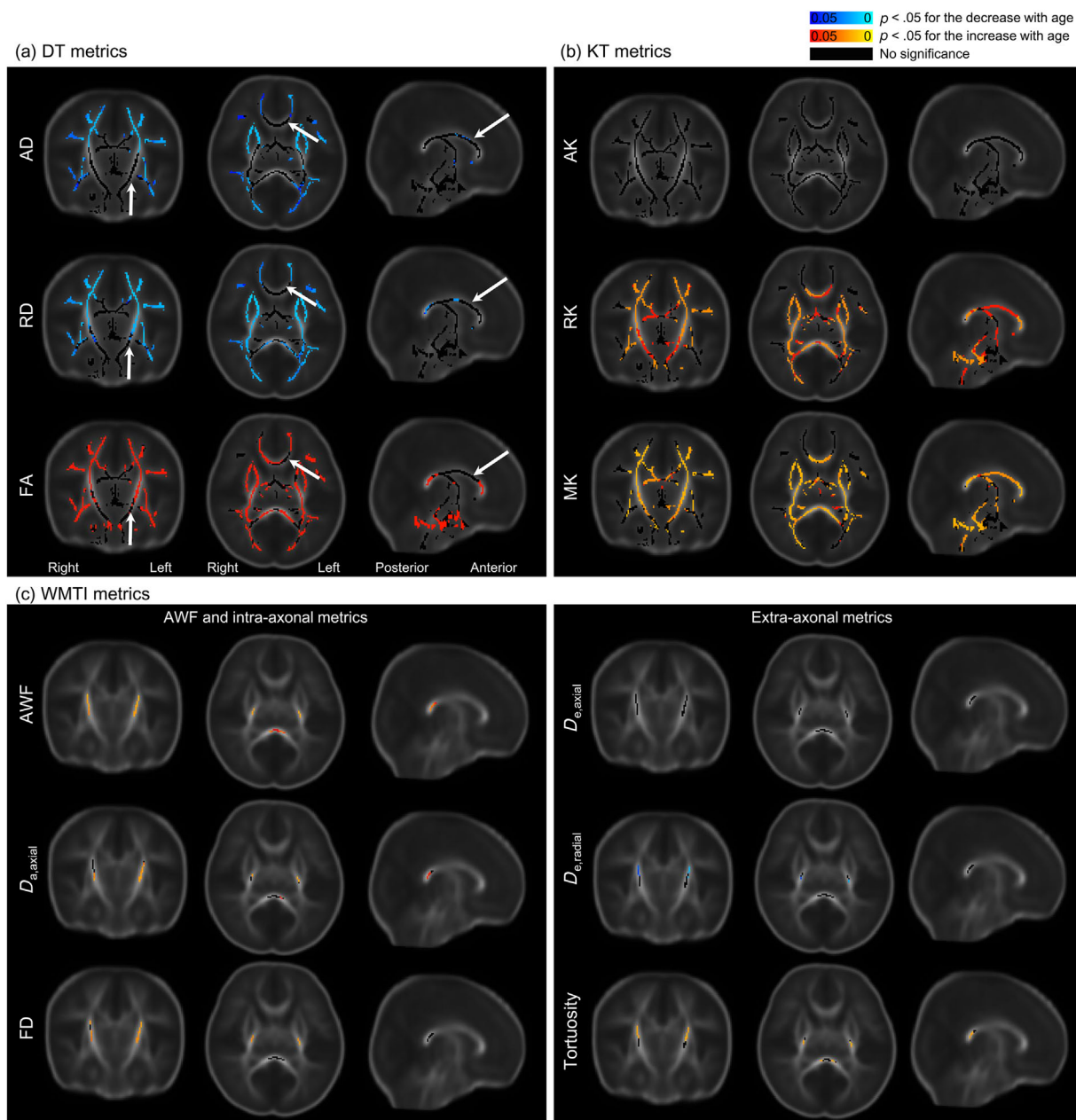
FIGURE 2 Postmenstrual age-related changes in DT (a), KT (b), and WMTI metrics (c) on white matter revealed by tract-based spatial statistics. The statistics are performed by using the general linear model while adjusting for covariates of the gender and the birth weight. DT, diffusion tensor; KT, kurtosis tensor; WMTI, white matter tract integrity

3.4.3 | Correlation with the neurobehavioral score

$D_{M,DT-KT}$ and $D_{M,DT}$ demonstrated significant negative correlation with the neurobehavioral score (Figure 7 and Figure S10). Both TBSS and ROI analyses showed that $D_{M,DT-KT}$ could reveal negative correlation in almost all the white matter regions except for right CST_CP, while $D_{M,DT}$ could only reveal the correlation on limited regions (e.g., right ILF) (Figure 7b). Furthermore, absolute values of correlation coefficients revealed by $D_{M,DT-KT}$ (r: −.28 to −.50) were higher than those revealed by $D_{M,DT}$ (r: −.11 to −.40) (Figure S10). Relatively stronger correlation could be found on ILF, anterior thalamic radiation, and left SLF (indicated by arrows in Figure 7a).

4 | DISCUSSION

This study investigated the performance of DKI with the multiparametric analysis in assessing white matter maturational processes and degrees on term neonates. KT and WMTI metrics provided additional PMA-related change patterns in comparison to DT metrics, which may be helpful for understanding maturational processes on neonatal white matter. Furthermore, KT metrics improved the performance of the Mahalanobis distance in quantifying maturational degrees. Compared with $D_{M,DT}$, $D_{M,DT-KT}$ demonstrated advantages in revealing correlations with PMA and the neurobehavioral score.
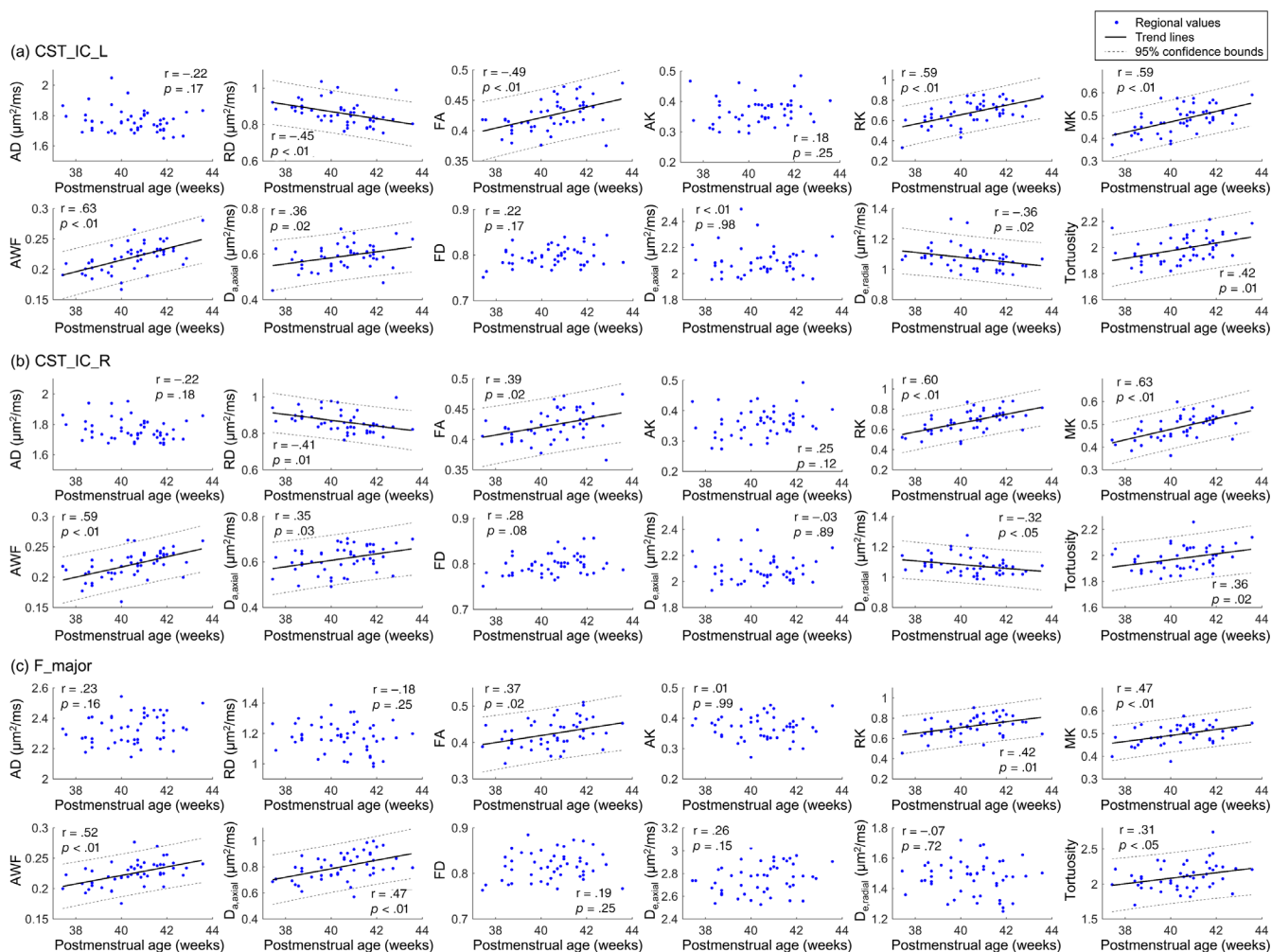
FIGURE 3 Scatter plots of metrics with the postmenstrual age in various regions of interest. For metrics with significant correlation with the postmenstrual age after controlling the gender and the birth weight, trend lines and 95% confidence intervals are added. Trend lines and 95% confidence intervals are not provided in plots without significant correlation. L, left; R, right

4.1 | Changes in derived metrics and maturational processes on neonatal white matter

Age-related changes in DT metrics in current work are in consistent with previous studies (Ball et al., 2010; Berman et al., 2005; Dubois et al., 2008; Geng et al., 2012; Kersbergen et al., 2014): increasing FA and decreasing AD and RD. This work also provided combinations of changes in different metrics (Figure 4): CST_IC and central part of the F_major mainly underwent increasing FA, unchanged AD and decreasing RD, while other regions mainly underwent increasing FA, synchronously decreasing AD and RD. Myelination is one of the factors influencing developmental changes in DT metrics. Postmortem studies suggest that the telencephalon starts myelination at the posterior limb of the internal capsule during the third trimester of gestation, while other tracts (e.g., corpus callosum) start myelination after birth (Brody, Kinney, Kloman, & Gilles, 1987; Kinney, Brody, Kloman, & Gilles, 1988). The electron microscopic analysis on the monkey corpus callosum suggests that at least 30% of axons in the posterior part are myelinated at the end of the first postnatal month (LaMantia &

Rakic, 1990). Additionally, demyelination or dysmyelination causes increased RD, but unchanged AD (Song et al., 2002; Song et al., 2005). Together with these postmortem findings, myelination may be the main factor causing developmentally increasing FA, unchanged AD and decreasing RD on CST_IC and central part of the F_major. However, the exact relationship between DT metrics and myelination is not clear due to the limited specificity of these metrics. Similar to previous findings (Dean III, Planalp, et al., 2017; Gilmore et al., 2007; Hüppi et al., 1998; Kunz et al., 2014), increased FA, accompanied with decreased AD and RD could be observed in unmyelinated regions (e.g., F_minor, ILF, and SLF). Prior to the myelination, premyelination characterized by the proliferation of oligodendrocytes has been assumed to be one of the main factors causing synchronously decreased AD and RD (Dubois et al., 2008, 2014; Ouyang, Jeon, et al., 2019). Although this combination pattern could be partly interpreted by the premyelination process, the cell proliferation and the myelin synthesis are difficult to be distinguished by DT metrics when they are overlapped during the same period (Geng et al., 2012). Additionally, increased AD has been observed during the fetal period,
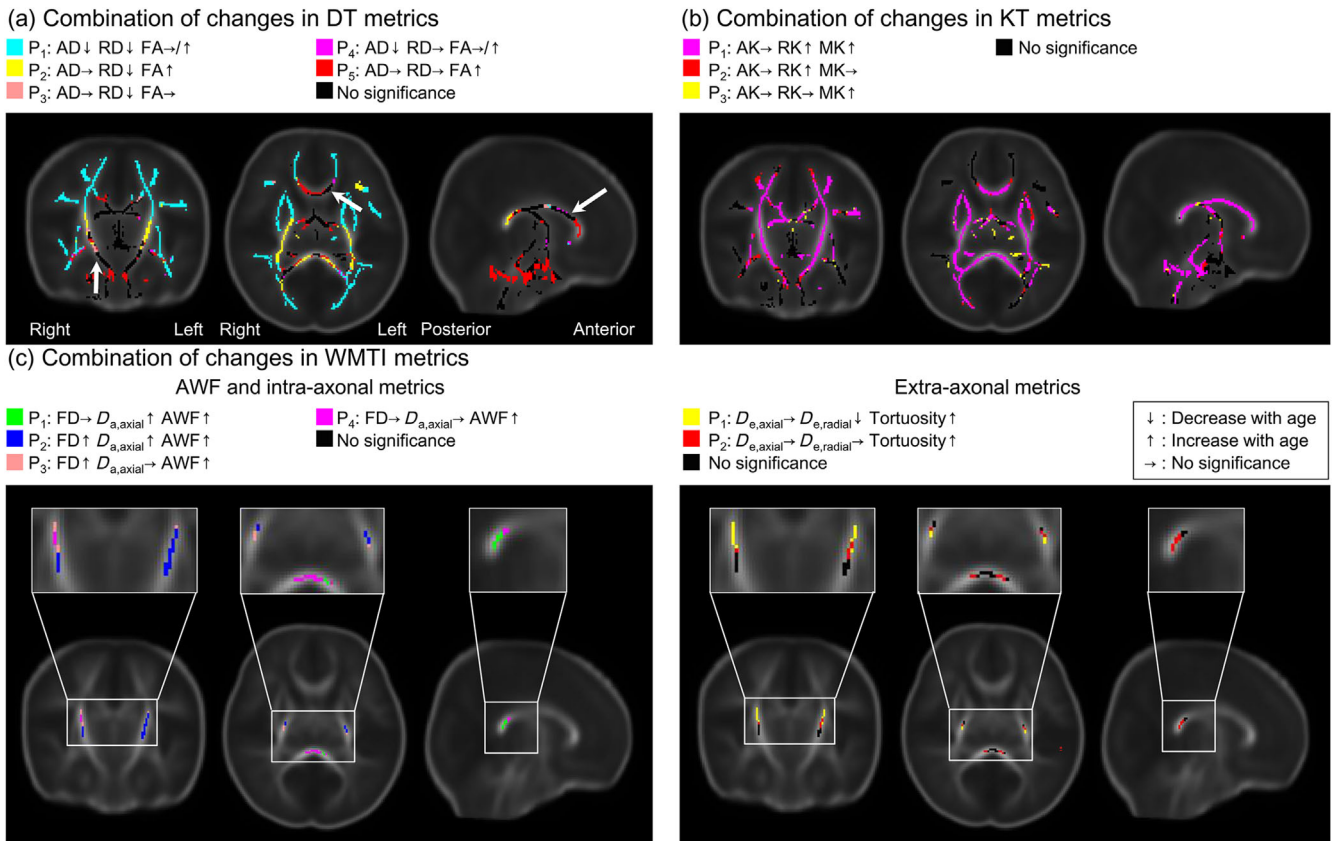
FIGURE 4 Combination patterns of postmenstrual age-related changes in DT (a), KT (b) and WMTI metrics (c). DT, diffusion tensor; KT, kurtosis tensor; WMTI, white matter tract integrity
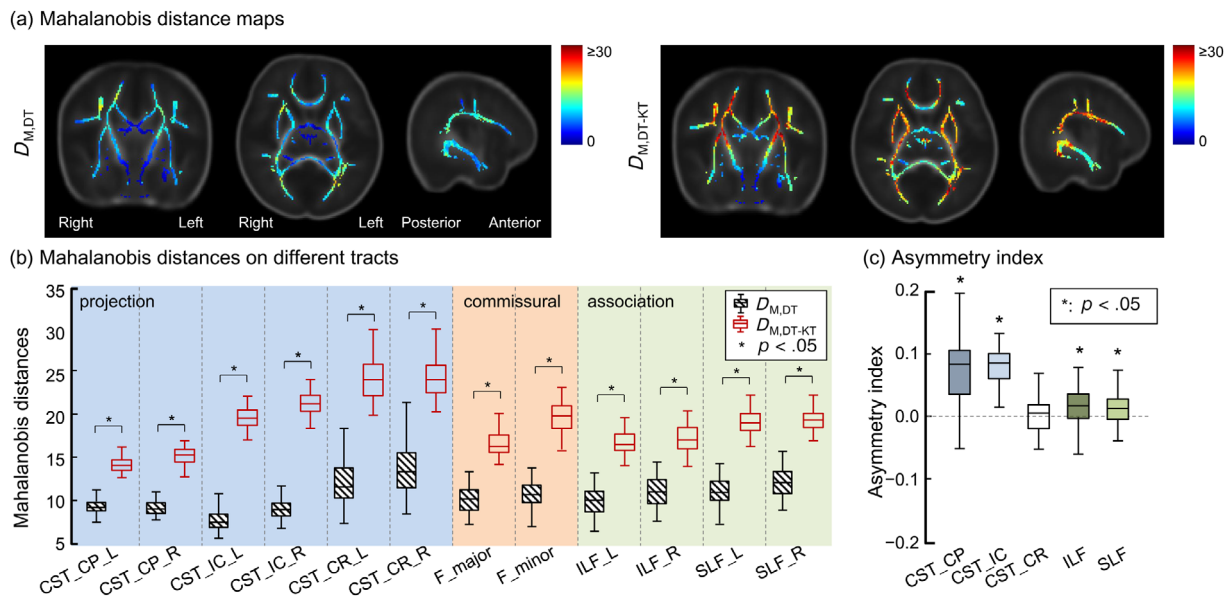
FIGURE 5 Median Mahalanobis distance maps (a), regional values of different white matter tracts (b), and asymmetry index on term neonates (c). DT, diffusion tensor; KT, kurtosis tensor; $D_{M,DT}$, Mahalanobis distances based on DT metrics; $D_{M,DT-KT}$, Mahalanobis distances based on the combination of DT and KT metrics; L, left; R, right

which may be related to the process of fiber organization (Zanin et al., 2011). Different from the maturation in the fetal period, the premyelination and/or myelination are intense during the first post-

natal month (Dubois et al., 2014), which would lead to rapid decreases in AD and RD. This may cover up the increase in AD corresponding to the process of the fiber organization (Dubois et al., 2008, 2014;

(a) Correlation with the postmenstrual age
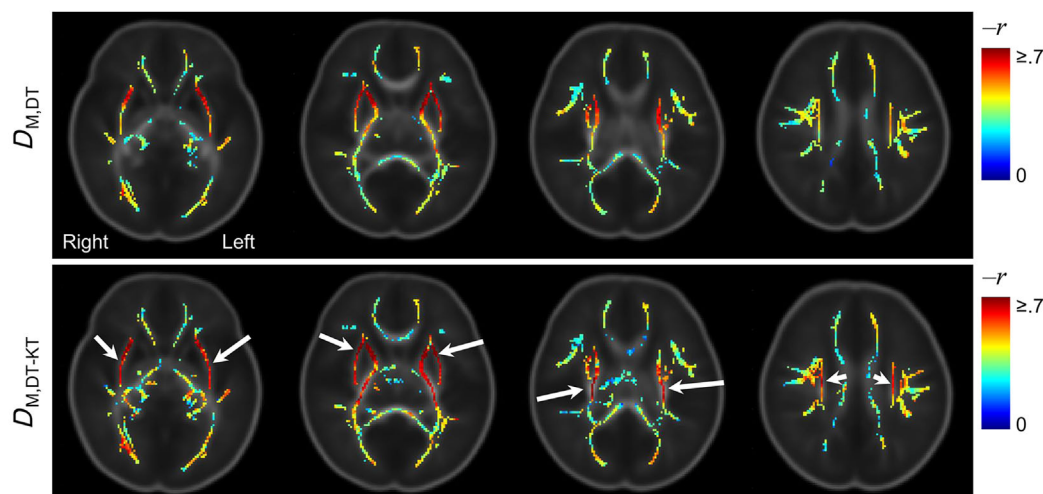
(b) Trend lines of changes with the postmenstrual age

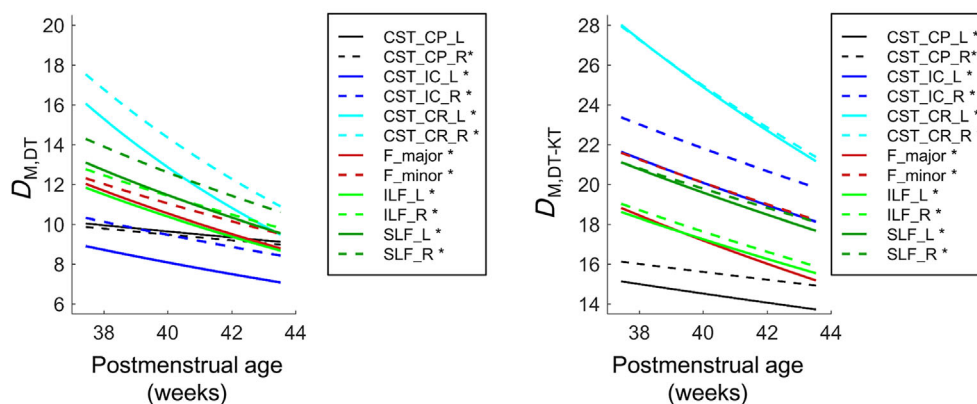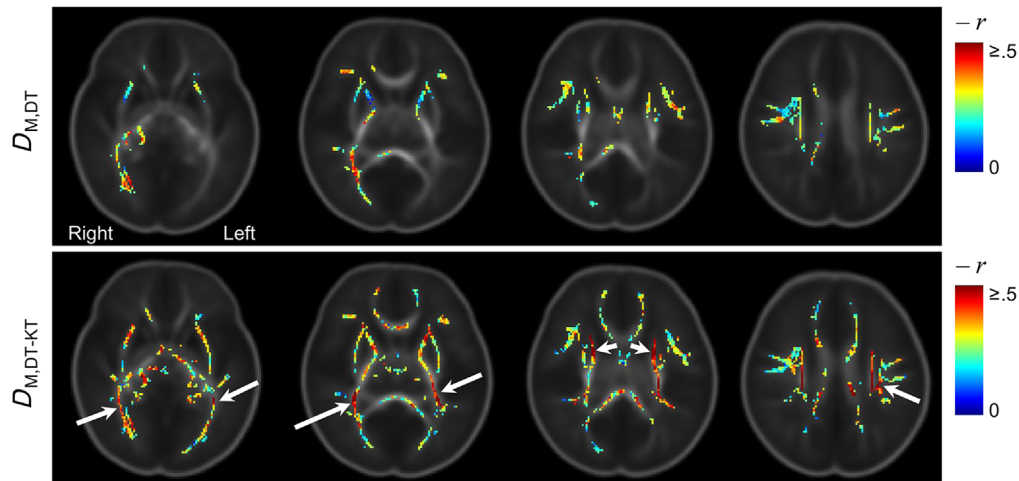**FIGURE 6** Correlation between Mahalanobis distances and the postmenstrual age on term neonates revealed by tract-based spatial statistics (a) and the region of interest analysis (b). Correlations are performed by using the partial Spearman correlation while controlling for effects of the gender and the birth weight. DT, diffusion tensor; KT, kurtosis tensor; $D_{M,DT}$, Mahalanobis distances based on DT metrics; $D_{M,DT-KT}$, Mahalanobis distances based on the combination of DT and KT metrics; r, correlation coefficient; L, left; R, right

Ouyang, Jeon, et al., 2019). Therefore, increasing AD was not observed during the neonatal period in this work.

In comparison with DT metrics, KT metrics could provide additional information for investigating white matter maturation (Cheung et al., 2009; Grinberg et al., 2017; Paydar et al., 2014). Consistent with previous studies, RK and MK demonstrated relatively higher sensitivity to structural changes in several white matter regions (e.g., CP and corpus callosum) of neonates. However, it is difficult to infer maturational processes just based on KT metrics due to the limited specificity (Fieremans et al., 2011). WMTI metrics are helpful for understanding more detailed maturation processes than DT and KT metrics (Jelescu et al., 2015). In the current work, AWF, $D_{a,axial}$, FD, tortuosity increased with PMA, while $D_{e,radial}$ decreased with PMA. Increased AWF may be related to the increase of the axonal packing density, resulting from axonal growth and/or myelination. The reduction of water content in the extra-axonal space during development is also a factor contributing to the increased AWF (Ouyang, Jeon, et al., 2019).

As for changes in $D_{a,axial}$, variation of the axonal structure could alter regional values of the intra-axonal diffusivity (Hui et al., 2012). During white matter maturation, neurofilaments are more organized mediated by the myelin-directed outside-in signaling cascade, in addition to the increased neighbor spacing of neurofilaments and the increased axoplasmic flow (Garcia et al., 2003; Suzuki et al., 2003). Meanwhile, the density of the microtubule and mitochondria also decreases with the axonal growth (Andrews et al., 2006; Garcia et al., 2003; Stassart et al., 2018). These alterations would reduce restrictions of diffusion along the axon, which may increase $D_{a,axial}$ (as shown in the Figure S11) (Garcia et al., 2003; Lee et al., 2020; Suzuki et al., 2003). Age-related increases in FD on neonates may be associated with increasing alignment of axons (Jelescu et al., 2015). As for changes in the extra-axonal compartment, myelination accompanied with decreases in the brain water content and increases in the concentration of macromolecules may be main factors leading to deceased $D_{e,radial}$ (Dubois et al., 2008; Ouyang, Jeon, et al., 2019). Changes of

(a) Correlation with the neurobehavioral score

(b) Trend lines of changes with the neurobehavioral score
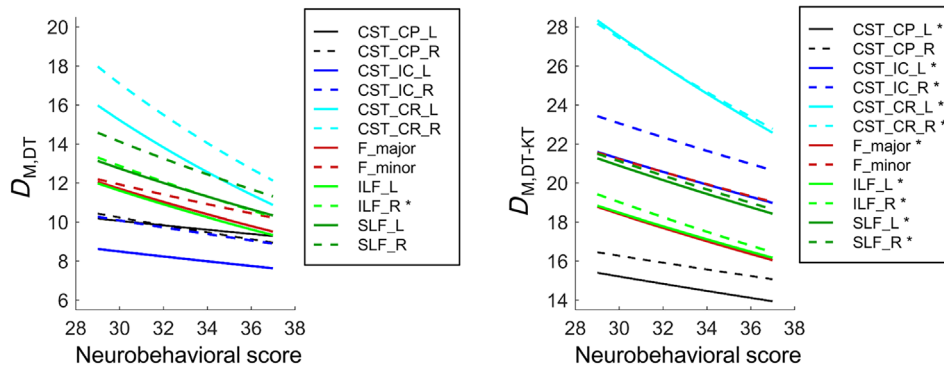
FIGURE 7 Correlation between Mahalanobis distances and the neurobehavioral score on term infants revealed by tract-based spatial statistics (a) and the region of interest analysis (b). Correlations are performed by using the partial Spearman correlation while controlling for effects of the postmenstrual age, the gender and the birth weight. DT, diffusion tensor; KT, kurtosis tensor; $D_{M,DT}$, Mahalanobis distances based on DT metrics; $D_{M,DT-KT}$, Mahalanobis distances based on the combination of DT and KT metrics; r, correlation coefficient; L, left; R, right

tortuosity may be associated with partly fiber organization and partly the enhancement of myelin sheath around axons (Dubois et al., 2014; Jelescu et al., 2015). Combinations of changes in DT, KT, and WMTI metrics would provide additional information for assessing maturational processes.

Although WMTI metrics have been used to assess white matter development on children aged 0–3 years old (Jelescu et al., 2015), the feasibility of WMTI on neonates remains to be validated (Fieremans et al., 2011). Various conditions should be considered. Firstly, the model is expected to be valid in regions with relatively aligned fibers and the angular spread of less than 30°. Secondly, the exchange between intra-axonal and extra-axonal spaces is neglected, which may be satisfied in regions containing myelinated axons due to the myelin sheath with very low permeability (Fieremans et al., 2011). The current work performed the analysis on the alignment-invariant tract representation (FA skeleton) (Smith et al., 2006) and restricted the analysis to voxels with FD ≥0.75 (corresponding to angle ≤30°) (Fieremans et al., 2011; Jelescu et al., 2015). As shown in the Figure S3, voxels with FD ≥0.75 mainly locate in the CST_IC and F_major. During the neonatal period,

these tracts hold a fraction of myelinated axons (Brody et al., 1987; Kinney et al., 1988; LaMantia & Rakic, 1990). Combined with the relatively small intersecting angle, the appearance of myelin sheath with low permeability makes modeling by WMTI possible (Fieremans et al., 2011). However, potential confounding factors should be taken into consideration for the interpretation of changes in WMTI metrics: As FD increased with PMA in CST_IC (Figure 2), more paralleled of fibers would be one of the factors increasing $D_{a,axial}$ (Jelescu et al., 2015). Meanwhile, there are also other confounding factors influencing alterations in $D_{a,axial}$. Caliber variation and/or undulation along the axon have been found to be related to changes of $D_{a,axial}$ (Lee et al., 2020). Additionally, considering that intra-axonal diffusivities would be underestimated due to the axonal membrane permeability, decreased permeability due to myelination in F_major would affect the interpretation of the increase in $D_{a,axial}$. Furthermore, although glial cells were found to have small volume fractions (~5%) (Veraart et al., 2020), there may possibly be a contribution to the intra-axonal space from glial processes. The proliferation and maturation of glial cells may also be another confounding factor.

4.2 | Mahalanobis distances and maturational degrees on neonatal white matter

For the interpretation of values in the Mahalanobis distance, several conditions should be considered: Firstly, the directionality of the distance depends on the selected reference. If the reference is the developing brain instead of the mature brain, values of distances in younger and older subjects could be the same, though the distance may also work to demonstrate developmental changes of neonatal white matter. In a previous study, developing controls serve as the reference (Dean III, Lange, et al., 2017). In this previous study, the Mahalanobis distance is used to reveal relative differences across groups instead of maturational degrees. Therefore, to interpret the distance as the maturational degree, the reference should be the mature brain. As age has impact on structural changes in the brain, adults in the plateau period may be candidates of the reference. It also depends on the type of measurements. For DT and KT metrics, changes reach a plateau in late adolescence or in the twenties (Das et al., 2017; Paydar et al., 2014; Tamnes et al., 2010). Secondly, the interpretation of the distance can also be influenced by the investigative age range. Though the mature brain is the reference, values of the distance may be interpreted as senescence if investigative participants are aged subjects. Another confounding factor is the direction of developmental changes of the enrolled metric during the Mahalanobis distance calculation. If the developmental change of the metric is not in one direction (e.g., inverted U trajectory for the cortical thickness: increasing in the early childhood and decreasing later), it is difficult to determine maturational degrees just based on values of distances. Therefore, the developmental change in each enrolled metric should be in one direction toward the reference. In this study, adults with age from 18.92 to 26.92 years were selected as the reference. The investigative participants were neonates. Developmental changes in each metric was in one direction toward the reference (Figures 1 and 2). According to these conditions, values of the Mahalanobis distance mainly reflect maturational degrees in the current work.

DKI is helpful to improve performances of the Mahalanobis distance in revealing correlations with PMA and the neurobehavioral score. Similar to results of the comparison between univariate and multivariate analyses (Dean III, Lange, et al., 2017; Kulikova et al., 2015), the dependency of the Mahalanobis distance on the metric selection was also found in this study. Compared with $D_{M,DT}$, $D_{M,DT-KT}$ revealed stronger negative correlations with PMA and the neurobehavioral score. Additionally, this current work demonstrated that including more metrics into the Mahalanobis distance calculation could not definitely improve its performances. Figure S6 showed that including MK could improve performances of the Mahalanobis distance, while including MD could not. This may be due to that MD can be fully determined by AD and RD. Different from MD, MK provides independent information from AK and RK (Nørhøj Jespersen, 2018). Previous DKI studies also find that KT metrics could offer more sensitive evaluation of the structural alterations during the brain maturation, in comparison with DT metrics (Cheung et al., 2009; Grinberg et al., 2017; Paydar et al., 2014). Specifically, DT metrics may provide information related to microstructure alterations related to the oligodendrocyte proliferation and myelination (Ouyang, Jeon, et al., 2019). Besides these developmental events, KT metrics are also sensitive to the diffusion heterogeneity associated with the axonal packing and/or diffusion barriers (Ouyang, Jeon, et al., 2019; Paydar et al., 2014). Results here further suggest that the improved sensitivity of the Mahalanobis distance would benefit the characterization of the maturation on developing brains.

The variation in regional values of $D_{M,DT-KT}$ demonstrates the asynchronous maturation across white matter tracts, which is in agreement with the myelination sequence (Brody et al., 1987; Kinney et al., 1988). As reported in previous studies (Brody et al., 1987; Deoni et al., 2011; Kinney et al., 1988), the cerebral peduncle holds higher maturational degree than other white matter tracts in the telencephalon. Therefore, CST_CP in this current study holds the lowest value of $D_{M,DT-KT}$ than other regions. Additionally, mature myelin can already be detected on neonates in the posterior limb of internal capsule (Dubois et al., 2014; Hasegawa et al., 1992). This supports the relatively lower Mahalanobis distances in CST_IC. Note that CST_CR holds the largest $D_{M,DT-KT}$ and high decreasing speed. These results confirm the previous finding that portions close to the cerebral cortex along the CST achieve a lower maturation degree than portions close to the cerebral peduncle on neonates (Geng et al., 2012). As for commissural tracts, F_major starts myelination from birth on, while F_minor starts myelination around 6 months of the postnatal age (Dubois et al., 2008, 2014). This sequence determines that F_major holds smaller $D_{M,DT-KT}$ than F_minor. Association tracts involved in the high-level processing always begin to myelinate at a relative late stage (Dubois et al., 2008, 2014). Therefore, relatively larger Mahalanobis distances can be found in ILF and SLF. Furthermore, regional values of $D_{M,DT-KT}$ in CST_CP, CST_IC, ILF, and SLF also demonstrate the inter-hemisphere asymmetry (i.e., left tracts hold lower Mahalanobis distances than the right, Figure 5c). Among the investigative tracts, CST is the major motor projection tract (Jaspers, Byblow, Feys, & Wenderoth, 2015). Asymmetry could be found on CST at the cerebral peduncles and the internal capsule levels, but not the corona radiata level. This may be related to the spatial spread of maturation over the CST (Dubois et al., 2009). ILF connects temporal and occipital lobes, related to functions of the visual modality, reading, lexical, and semantic processing (Herbet, Zemmoura, & Duffau, 2018). SLF connects frontal, occipital, parietal, and temporal lobes, associated with attention and language (Urger et al., 2015). The leftward asymmetry in $D_{M,DT-KT}$ of these tracts may be associated with the development of functional lateralization of motor and language (Dubois et al., 2009). The lateralized specialization has been thought to originate from evolutionary, developmental, hereditary, experiential, and pathological factors (Toga & Thompson, 2003). Two-thirds of fetuses are confined to a leftward fetal position in the third trimester (Previc, 1991). The asymmetrical vestibular stimulation in utero might produce behavioral asymmetries later in life (Previc, 1991). Moreover, the neonatal brain has demonstrated leftward asymmetric efficiency at both global and local levels (Ratnarajah et al., 2013). Specifically, left

precentral gyrus holds more efficient communications than the right homolog. Intercolumn connections are less tangled and more myelinated on the left than the right in auditory cortex (Warrier et al., 2009). Therefore, the left lateralization of the neonatal white matter maturation may be partly a result of the adaption to lateralized functional needs at birth (Ratnarajah et al., 2013).

White matter maturation has been found to correspond with the development of neurobehavioral abilities in previous studies (Bassi et al., 2008; George et al., 2018; Jin et al., 2019; Kelly et al., 2019). Specifically, the structural maturation of optic radiation, corona radiate, and corpus callosum on newborns is associated with visual, motor, and cognitive outcomes, respectively (Bassi et al., 2008; Kaukola et al., 2010; Thompson et al., 2012). In this current work, the neurobehavioral score reflects comprehensively the ability to interact with the environment (Bao et al., 1991). Negative correlations between $D_{M,DT-KT}$ and the neurobehavioral score can be found in almost all the white matter regions. Among the investigative white matter tracts, ILF, anterior thalamic radiation, and left SLF hold relatively stronger correlation with the neurobehavioral score (Figure 7a). This may be related to the high order functions (e.g., the visual modality, attention, and language) of these tracts associated closely with the neurobehavioral ability (Herbet et al., 2018; Urger et al., 2015). Importantly, $D_{M,DT-KT}$ demonstrated advantages than $D_{M,DT}$ in revealing the correlation with the neurobehavioral score. Results in this work further suggest that $D_{M,DT-KT}$ may serve as an objective metric to reveal maturational degrees associated with neurobehavioral abilities.

4.3 | Limitations

Nevertheless, there are some limitations in this current study. Firstly, this is a cross-sectional study. Further longitudinal study is needed to confirm maturational processes revealed in this work. Secondly, the finally enrolled neonates were sedated, as the natural sleep neonates were excluded due to motion artifacts. Although structural properties are not theoretically influenced by the sedation (Cavaliere et al., 2015), diffusion MRI metrics here should be interpreted under the sedation condition. Thirdly, diffusion MRI metrics are sensitive to various maturational processes (Alexander et al., 2011; Alexander, Lee, Lazar, & Field, 2007; Dubois et al., 2014; Jones et al., 2013; Jones & Cercignani, 2010; Ouyang, Jeon, et al., 2019). Although WMTI metrics offer relatively more specific than DT metrics, mapping diffusion metrics onto specific maturational processes is still a difficult inverse problem (Jones et al., 2013). Therefore, changes in diffusion metrics should be interpreted with caution (Alexander et al., 2007, 2011; Jones et al., 2013; Jones & Cercignani, 2010). Additionally, this study demonstrated maturation only on FA skeleton instead of the whole brain, as the voxel-based analysis for the whole brain faces problems caused by alignment inaccuracies and the lack of a principled way for choosing smoothing extent (Smith et al., 2006). And the analysis for WMTI metrics was performed on voxels with FD ≥0.75 (corresponding to angle ≤30°) due to WMTI model assumptions (Fieremans et al., 2011). Other regions remain to be investigated. The

acquisition voxel resolution in this study is not isotropic. This is another limitation that may lead to underestimated parametric values in areas with crossing fibers (Chiang et al., 2019; Ooucchi et al., 2007). Furthermore, this study calculated the Mahalanobis distance based on DT and KT metrics. In fact, the Mahalanobis distance framework can also include other metrics (Kulikova et al., 2015). During further applications, it is better to take more independent metrics into consideration to fully reflect the brain maturation. Besides the Mahalanobis distance, several other strategies (e.g., multiview clustering, indefiniteness elimination network, etc.) have also been proposed for multimodality and/or multidimension analyses (Guo, Liu, Zhao, Guo, & Liu, 2021; Li et al., 2019; Osman, 2019; Zhao et al., 2015). The indefiniteness elimination network has achieved impressing performance to transfer the indefinite dimension feature into a fixed dimension feature (Guo et al., 2021). In the future, the deep learning-based strategy combining with multimodality and clinical items may further improve our ability to characterize the brain maturation.

5 | CONCLUSIONS

In conclusion, this work demonstrates the application of DKI with the multiparametric analysis to characterize white matter maturational processes and degrees on term neonates. Combinations of changes in DT, KT, and WMTI metrics provide additional information for assessing maturational processes. KT metrics could improve the performance of the Mahalanobis distance in quantifying maturational degrees. Results in current work would further benefit our understanding on white matter maturation of term neonates.

CONFLICT OF INTEREST
The authors declare that there are no financial or other relationships that might lead to a conflict of interest.

ETHICS STATEMENT
This study was approved by the local institutional review board. Informed written consents were obtained from adult participants and parents of neonates.

DATA AVAILABILITY STATEMENT
The data was available from the corresponding author upon reasonable request.

ORCID
Xianjun Li https://orcid.org/0000-0001-7690-9155
Heng Liu https://orcid.org/0000-0002-6108-5154
Jian Yang https://orcid.org/0000-0003-4250-1391

REFERENCES

Alexander, A. L., Hurley, S. A., Samsonov, A. A., Adluru, N., Hosseinbor, A. P., Mossahebi, P., ... Field, A. S. (2011). Characterization of cerebral white matter properties using quantitative magnetic resonance imaging stains. *Brain Connectivity*, *1*(6), 423–446.

Alexander, A. L., Lee, J. E., Lazar, M., & Field, A. S. (2007). Diffusion tensor imaging of the brain. *Neurotherapeutics*, *4*(3), 316–329.

Amiel-Tison, C., Barrier, G., Shnider, S. M., Levinson, G., Hughes, S. C., & Stefani, S. J. (1982). A new neurologic and adaptive capacity scoring system for evaluating obstetric medications in full-term newborns. *Anesthesiology*, *56*(5), 340–350.

Andrews, H., White, K., Thomson, C., Edgar, J., Bates, D., Griffiths, I., ... Nichols, P. (2006). Increased axonal mitochondrial activity as an adaptation to myelin deficiency in the Shiverer mouse. *Journal of Neuroscience Research*, *83*(8), 1533–1539.

Ball, G., Counsell, S. J., Anjari, M., Merchant, N., Arichi, T., Doria, V., ... Boardman, J. P. (2010). An optimised tract-based spatial statistics protocol for neonates: Applications to prematurity and chronic lung disease. *NeuroImage*, *53*(1), 94–102.

Bao, X. L., Yu, R. J., Li, Z. S., & Zhang, B. L. (1991). Twenty-item behavioral neurological assessment for normal newborns in 12 cities of China. *Chinese Medical Journal*, *104*(9), 742–746.

Bassi, L., Ricci, D., Volzone, A., Allsop, J. M., Srinivasan, L., Pai, A., ... Counsell, S. J. (2008). Probabilistic diffusion tractography of the optic radiations and visual function in preterm infants at term equivalent age. *Brain*, *131*(Pt 2), 573–582.

Berman, J. I., Mukherjee, P., Partridge, S. C., Miller, S. P., Ferriero, D. M., Barkovich, A. J., ... Henry, R. G. (2005). Quantitative diffusion tensor MRI fiber tractography of sensorimotor white matter development in premature infants. *NeuroImage*, *27*(4), 862–871.

Brazelton, T. B. (1984). *Neonatal behavioral assessment scale* (2nd ed., pp. 1–104). Philadelphia, PA: JB Lippincott.

Brody, B. A., Kinney, H. C., Kloman, A. S., & Gilles, F. H. (1987). Sequence of central nervous system myelination in human infancy. I. an autopsy study of myelination. *Journal of Neuropathology & Experimental Neurology*, *46*(3), 283–301.

Cavaliere, C., Aiello, M., Di Perri, C., Fernandez-Espejo, D., Owen, A. M., & Soddu, A. (2015). Diffusion tensor imaging and white matter abnormalities in patients with disorders of consciousness. *Frontiers in Human Neuroscience*, *8*, 1028.

Cheung, M. M., Hui, E. S., Chan, K. C., Helpern, J. A., Qi, L., & Wu, E. X. (2009). Does diffusion kurtosis imaging lead to better neural tissue characterization? A rodent brain maturation study. *NeuroImage*, *45*(2), 386–392.

Chiang, C. W., Lin, S. Y., Cho, K. H., Wu, K. J., Wang, Y., & Kuo, L. W. (2019). Effects of signal averaging, gradient encoding scheme, and spatial resolution on diffusion kurtosis imaging: An empirical study using 7T MRI. *Journal of Magnetic Resonance Imaging*, *50*(5), 1593–1603.

Coté, C. J., & Wilson, S. (2006). Guidelines for monitoring and management of pediatric patients during and after sedation for diagnostic and therapeutic procedures: An update. *Pediatrics*, *118*(6), 2587–2602.

Das, S. K., Wang, J. L., Bing, L., Bhetuwal, A., & Yang, H. F. (2017). Regional values of diffusional kurtosis estimates in the healthy brain during normal aging. *Clinical Neuroradiology*, *27*(3), 283–298.

Dean, D. C., III, Lange, N., Travers, B. G., Prigge, M. B., Matsunami, N., Kellett, K. A., ... Tromp, D. P. M. (2017). Multivariate characterization of white matter heterogeneity in autism spectrum disorder. *Neuroimage: Clinical*, *14*(1), 54–66.

Dean, D. C., III, Planalp, E. M., Wooten, W., Adluru, N., Kecskemeti, S. R., Frye, C., ... Alexander, A. L. (2017). Mapping white matter microstructure in the one month human brain. *Scientific Reports*, *7*(1), 9759.

Deoni, S. C. L., Mercure, E., Blasi, A., Gasston, D., Thomson, A., Johnson, M., ... Murphy, D. G. M. (2011). Mapping infant brain myelination with magnetic resonance imaging. *The Journal of Neuroscience*, *31*(2), 784–791.

Dubois, J., Dehaene-Lambertz, G., Kulikova, S., Poupon, C., Hüppi, P. S., & Hertz-Pannier, L. (2014). The early development of brain white matter: A review of imaging studies in fetuses, newborns and infants. *Neuroscience*, *276*(6), 48–71.

Dubois, J., Dehaene-Lambertz, G., Perrin, M., Mangin, J.-F., Cointepas, Y., Duchesnay, E., ... Hertz-Pannier, L. (2008). Asynchrony of the early maturation of white matter bundles in healthy infants: Quantitative landmarks revealed noninvasively by diffusion tensor imaging. *Human Brain Mapping*, *29*(1), 14–27.

Dubois, J., Hertz-Pannier, L., Cachia, A., Mangin, J. F., Le Bihan, D., & Dehaene-Lambertz, G. (2009). Structural asymmetries in the infant language and sensori-motor networks. *Cerebral Cortex*, *19*(2), 414–423.

Fieremans, E., Jensen, J. H., & Helpern, J. A. (2011). White matter characterization with diffusional kurtosis imaging. *NeuroImage*, *58*(1), 177–188.

Garcia, M. L., Lobsiger, C. S., Shah, S. B., Deerinck, T. J., Crum, J., Young, D., ... Cleveland, D. W. (2003). NF-M is an essential target for the myelin-directed "outside-in" signaling cascade that mediates radial axonal growth. *The Journal of Cell Biology*, *163*(5), 1011–1020.

Geng, X., Gouttard, S., Sharma, A., Gu, H., Styner, M., Lin, W., ... Gilmore, J. H. (2012). Quantitative tract-based white matter development from birth to age 2 years. *NeuroImage*, *61*(3), 542–557.

George, J. M., Fiori, S., Fripp, J., Pannek, K., Guzzetta, A., David, M., ... Boyd, R. N. (2018). Relationship between very early brain structure and neuromotor, neurological and neurobehavioral function in infants born <31 weeks gestational age. *Early Human Development*, *117*, 74–82.

Ghorbani, H. (2019). Mahalanobis distance and its application for detecting multivariate outliers. *Facta Universitatis, Series: Mathematics and Informatics*, *34*(3), 583–595.

Gilmore, J. H., Knickmeyer, R. C., & Gao, W. (2018). Imaging structural and functional brain development in early childhood. *Nature Reviews. Neuroscience*, *19*(3), 123–137.

Gilmore, J. H., Lin, W., Corouge, I., Vetsa, Y. S., Smith, J. K., Kang, C., ... Gerig, G. (2007). Early postnatal development of corpus callosum and corticospinal white matter assessed with quantitative tractography. *AJNR: American Journal of Neuroradiology*, *28*(9), 1789–1795.

Grinberg, F., Maximov, I. I., Farrher, E., Neuner, I., Amort, L., Thönneßen, H., ... Shah, N. J. (2017). Diffusion kurtosis metrics as biomarkers of microstructural development: A comparative study of a group of children and a group of adults. *Neuroimage*, *144*, 12–22.

Guo, G., Liu, Z., Zhao, S., Guo, L., & Liu, T. (2021). Eliminating indefiniteness of clinical spectrum for better screening COVID-19. *IEEE Journal of Biomedical and Health Informatics*, *25*(5), 1347–1357.

Hasegawa, M., Houdou, S., Mito, T., Takashima, S., Asanuma, K., & Ohno, T. (1992). Development of myelination in the human fetal and infant cerebrum: A myelin basic protein immunohistochemical study. *Brain & Development*, *14*(1), 1–6.

Herbet, G., Zemmoura, I., & Duffau, H. (2018). Functional anatomy of the inferior longitudinal fasciculus: From historical reports to current hypotheses. *Frontiers in Neuroanatomy*, *12*, 77.

Hui, E. S., Fieremans, E., Jensen, J. H., Tabesh, A., Feng, W., Bonilha, L., ... Helpern, J. A. (2012). Stroke assessment with diffusional kurtosis imaging. *Stroke*, *43*(11), 2968–2973.

Hüppi, P. S., Maier, S. E., Peled, S., Zientara, G. P., Barnes, P. D., Jolesz, F. A., & Volpe, J. J. (1998). Microstructural development of human newborn cerebral white matter assessed in vivo by diffusion tensor magnetic resonance imaging. *Pediatric Research*, *44*(4), 584–590.

Jaspers, E., Byblow, W. D., Feys, H., & Wenderoth, N. (2015). The corticospinal tract: A biomarker to categorize upper limb functional potential in unilateral cerebral palsy. *Frontiers in Pediatrics*, *3*(1), 112.

Jelescu, I. O., Veraart, J., Adisetiyo, V., Milla, S. S., Novikov, D. S., & Fieremans, E. (2015). One diffusion acquisition and different white

matter models: How does microstructure change in human early development based on WMTI and NODDI? *NeuroImage*, 107, 242–256.

Jenkinson, M., Beckmann, C. F., Behrens, T. E., Woolrich, M. W., & Smith, S. M. (2012). FSL. *Neuroimage*, 62(2), 782–790.

Jin, C., Li, Y., Li, X., Wang, M., Liu, C., Gao, J., … Yang, J. (2019). Proper timing for the evaluation of neonatal brain white matter development: A diffusion tensor imaging study. *European Radiology*, 29(3), 1527–1537.

Jones, D. K., & Cercignani, M. (2010). Twenty-five pitfalls in the analysis of diffusion MRI data. *NMR in Biomedicine*, 23(7), 803–820.

Jones, D. K., Knösche, T. R., & Turner, R. (2013). White matter integrity, fiber count, and other fallacies: The do's and don'ts of diffusion MRI. *NeuroImage*, 73, 239–254.

Kaukola, T., Perhomaa, M., Vainionpaa, L., Tolonen, U., Jauhiainen, J., Paakko, E., & Hallman, M. (2010). Apparent diffusion coefficient on magnetic resonance imaging in pons and in corona radiata and relation with the neurophysiologic measurement and the outcome in very preterm infants. *Neonatology*, 97(1), 15–21.

Kelly, C. E., Thompson, D. K., Cheong, J. L., Chen, J., Olsen, J. E., Eeles, A. L., … Spittle, A. J. (2019). Brain structure and neurological and behavioural functioning in infants born preterm. *Developmental Medicine and Child Neurology*, 61(7), 820–831.

Kersbergen, K. J., Leemans, A., Groenendaal, F., van der Aa, N. E., Viergever, M. A., de Vries, L. S., & Benders, M. (2014). Microstructural brain development between 30 and 40 weeks corrected age in a longitudinal cohort of extremely preterm infants. *NeuroImage*, 103, 214–224.

Kinney, H. C., Brody, B. A., Kloman, A. S., & Gilles, F. H. (1988). Sequence of central nervous system myelination in human infancy. II. Patterns of myelination in autopsied infants. *Journal of Neuropathology & Experimental Neurology*, 47(3), 217–234.

Kulikova, S., Hertzpannier, L., Dehaenelambertz, G., Buzmakov, A., Poupon, C., & Dubois, J. (2015). Multi-parametric evaluation of the white matter maturation. *Brain Structure & Function*, 220(6), 3657–3672.

Kunz, N., Zhang, H., Vasung, L., O'Brien, K. R., Assaf, Y., Lazeyras, F., … Hüppi, P. S. (2014). Assessing white matter microstructure of the newborn with multi-shell diffusion MRI and biophysical compartment models. *NeuroImage*, 96(1), 288–299.

LaMantia, A. S., & Rakic, P. (1990). Axon overproduction and elimination in the corpus callosum of the developing rhesus monkey. *The Journal of Neuroscience*, 10(7), 2156–2175.

Lee, H. H., Papaioannou, A., Kim, S. L., Novikov, D. S., & Fieremans, E. (2020). A time-dependent diffusion MRI signature of axon caliber variations and beading. *Communications Biology*, 3(1), 354.

Li, C., Wang, S., Serra, A., Torheim, T., Yan, J. L., Boonzaier, N. R., … Price, S. J. (2019). Multi-parametric and multi-regional histogram analysis of MRI: Modality integration reveals imaging phenotypes of glioblastoma. *European Radiology*, 29(9), 4718–4729.

Li, X., Gao, J., Wang, M., Wan, M., & Yang, J. (2016). Rapid and reliable tract-based spatial statistics pipeline for diffusion tensor imaging in the neonatal brain: Applications to the white matter development and lesions. *Magnetic Resonance Imaging*, 34(9), 1314–1321.

Li, X., Yang, J., Gao, J., Luo, X., Zhou, Z., Hu, Y., … Wan, M. (2014). A robust post-processing workflow for datasets with motion artifacts in diffusion kurtosis imaging. *PLoS One*, 9(4), e94592.

Lindemer, E. R., Salat, D. H., Smith, E. E., Nguyen, K., Fischl, B., & Greve, D. N. (2015). White matter signal abnormality quality differentiates mild cognitive impairment that converts to Alzheimer's disease from nonconverters. *Neurobiology of Aging*, 36(9), 2447–2457.

Maesschalck, R. D., Jouan-Rimbaud, D., & Massart, D. L. (2000). The Mahalanobis distance. *Chemometrics and Intelligent Laboratory Systems*, 50(1), 1–18.

Nørhøj Jespersen, S. (2018). White matter biomarkers from diffusion MRI. *Journal of Magnetic Resonance*, 291(1), 127–140.

Oishi, K., Mori, S., Donohue, P. K., Ernst, T., Anderson, L., Buchthal, S., … Chang, L. (2011). Multi-contrast human neonatal brain atlas: Application to normal neonate development analysis. *NeuroImage*, 56(1), 8–20.

Oouchi, H., Yamada, K., Sakai, K., Kizu, O., Kubota, T., Ito, H., & Nishimura, T. (2007). Diffusion anisotropy measurement of brain white matter is affected by voxel size: Underestimation occurs in areas with crossing fibers. *AJNR: American Journal of Neuroradiology*, 28(6), 1102–1106.

Osman, A. F. I. (2019). A multi-parametric MRI-based radiomics signature and a practical ML model for stratifying glioblastoma patients based on survival toward precision oncology. *Frontiers in Computational Neuroscience*, 13, 58.

Ouyang, M., Dubois, J., Yu, Q., Mukherjee, P., & Huang, H. (2019). Delineation of early brain development from fetuses to infants with diffusion MRI and beyond. *NeuroImage*, 185, 836–850.

Ouyang, M., Jeon, T., Sotiras, A., Peng, Q., Mishra, V., Halovanic, C., … Huang, H. (2019). Differential cortical microstructural maturation in the preterm human brain with diffusion kurtosis and tensor imaging. *Proceedings of the National Academy of Sciences of the United States of America*, 116(10), 4681–4688.

Paus, T. (2010). Growth of white matter in the adolescent brain: Myelin or axon? *Brain and Cognition*, 72(1), 26–35.

Paydar, A., Fieremans, E., Nwankwo, J. I., Lazar, M., Sheth, H. D., Adisetiyo, V., … Milla, S. S. (2014). Diffusional kurtosis imaging of the developing brain. *AJNR. American Journal of Neuroradiology*, 35(4), 808–814.

Previc, F. H. (1991). A general theory concerning the prenatal origins of cerebral lateralization in humans. *Psychological Review*, 98(3), 299–334.

Ratnarajah, N., Rifkin-Graboi, A., Fortier, M. V., Chong, Y. S., Kwek, K., Saw, S. M., … Qiu, A. (2013). Structural connectivity asymmetry in the neonatal brain. *NeuroImage*, 75, 187–194.

Shehzad, Z., Kelly, C., Reiss, P. T., Cameron Craddock, R., Emerson, J. W., McMahon, K., … Milham, M. P. (2014). A multivariate distance-based analytic framework for connectome-wide association studies. *Neuroimage*, 93, 74–94.

Shi, F., Yap, P. T., Wu, G., Jia, H., Gilmore, J. H., Lin, W., & Shen, D. (2011). Infant brain atlases from neonates to 1- and 2-year-olds. *PLoS One*, 6(4), e18746.

Smith, S. M. (2002). Fast robust automated brain extraction. *Human Brain Mapping*, 17(3), 143–155.

Smith, S. M., Jenkinson, M., Johansen-Berg, H., Rueckert, D., Nichols, T. E., Mackay, C. E., … Behrens, T. E. J. (2006). Tract-based spatial statistics: Voxelwise analysis of multi-subject diffusion data. *NeuroImage*, 31(4), 1487–1505.

Smith, S. M., & Nichols, T. E. (2009). Threshold-free cluster enhancement: Addressing problems of smoothing, threshold dependence and localisation in cluster inference. *NeuroImage*, 44(1), 83–98.

Somerville, L. H. (2016). Searching for signatures of brain maturity: What are we searching for? *Neuron*, 92(6), 1164–1167.

Song, S. K., Sun, S. W., Ramsbottom, M. J., Chang, C., Russell, J., & Cross, A. H. (2002). Dysmyelination revealed through MRI as increased radial (but unchanged axial) diffusion of water. *NeuroImage*, 17(3), 1429–1436.

Song, S. K., Yoshino, J., Le, T. Q., Lin, S. J., Sun, S. W., Cross, A. H., & Armstrong, R. C. (2005). Demyelination increases radial diffusivity in corpus callosum of mouse brain. *NeuroImage*, 26(1), 132–140.

Stassart, R. M., Möbius, W., Nave, K. A., & Edgar, J. M. (2018). The axon-myelin unit in development and degenerative disease. *Frontiers in Neuroscience*, 12, 467.

Suzuki, K. (2007). Neuropathology of developmental abnormalities. *Brain Development*, 29(3), 129–141.

Suzuki, Y., Matsuzawa, H., Kwee, I. L., & Nakada, T. (2003). Absolute eigen-value diffusion tensor analysis for human brain maturation. *NMR in Biomedicine*, *16*(5), 257–260.

Tabesh, A., Jensen, J. H., Ardekani, B. A., & Helpern, J. A. (2011). Estimation of tensors and tensor-derived measures in diffusional kurtosis imaging. *Magnetic Resonance in Medicine*, *65*(3), 823–836.

Tamnes, C. K., Ostby, Y., Fjell, A. M., Westlye, L. T., Due-Tønnessen, P., & Walhovd, K. B. (2010). Brain maturation in adolescence and young adulthood: Regional age-related changes in cortical thickness and white matter volume and microstructure. *Cerebral Cortex*, *20*(3), 534–548.

Thompson, D. K., Inder, T. E., Faggian, N., Warfield, S. K., Anderson, P. J., Doyle, L. W., & Egan, G. F. (2012). Corpus callosum alterations in very preterm infants: Perinatal correlates and 2 year neurodevelopmental outcomes. *NeuroImage*, *59*(4), 3571–3581.

Toga, A. W., & Thompson, P. M. (2003). Mapping brain asymmetry. *Nature Reviews. Neuroscience*, *4*(1), 37–48.

Urger, S. E., De Bellis, M. D., Hooper, S. R., Woolley, D. P., Chen, S. D., & Provenzale, J. (2015). The superior longitudinal fasciculus in typically developing children and adolescents: Diffusion tensor imaging and neuropsychological correlates. *Journal of Child Neurology*, *30*(1), 9–20.

Veraart, J., Nunes, D., Rudrapatna, U., Fieremans, E., Jones, D. K., Novikov, D. S., & Shemesh, N. (2020). Nonivasive quantification of axon radii using diffusion MRI. *eLife*, *9*, e49855.

Veraart, J., Poot, D. H. J., Van Hecke, W., Blockx, I., Van der Linden, A., Verhoye, M., & Sijbers, J. (2011). More accurate estimation of diffusion tensor parameters using diffusion kurtosis imaging. *Magnetic Resonance in Medicine*, *65*(1), 138–145.

Warrier, C., Wong, P., Penhune, V., Zatorre, R., Parrish, T., Abrams, D., & Kraus, N. (2009). Relating structure to function: Heschl's gyrus and acoustic processing. *The Journal of Neuroscience*, *29*(1), 61–69.

Winkler, A. M., Ridgway, G. R., Webster, M. A., Smith, S. M., & Nichols, T. E. (2014). Permutation inference for the general linear model. *NeuroImage*, *92*(100), 381–397.

Zanin, E., Ranjeva, J. P., Confort-Gouny, S., Guye, M., Denis, D., Cozzone, P. J., & Girard, N. (2011). White matter maturation of normal human fetal brain. An in vivo diffusion tensor tractography study. *Brain and Behavior: A Cognitive Neuroscience Perspective*, *1*(2), 95–108.

Zhang, H., Schneider, T., Wheeler-Kingshott, C. A., & Alexander, D. C. (2012). NODDI: Practical in vivo neurite orientation dispersion and density imaging of the human brain. *NeuroImage*, *61*(4), 1000–1016.

Zhao, S., Han, J., Lv, J., Jiang, X., Hu, X., Zhao, Y., ... Liu, T. (2015). Supervised dictionary learning for inferring concurrent brain networks. *IEEE Transactions on Medical Imaging*, *34*(10), 2036–2045.

SUPPORTING INFORMATION

Additional supporting information may be found in the online version of the article at the publisher's website.